SCIENCE CHINA
Earth Sciences

•ARTICLE•

June 2024 Vol.67 No.6: 2019–2033
https://doi.org/10.1007/s11430-023-1275-2

Erosion-induced recovery CO_2 sink offset the horizontal soil organic carbon removal at the basin scale

Lingxia WANG[3], Xiaodong NIE[1,2*], Jiaqi LI[1], Yaojun LIU[1,2], Hui WANG[3], Yazhe LI[1] & Zhongwu LI[1,2,3*]

[1] *School of Geographic Science, Hunan Normal University, Changsha 410081, China;*
[2] *Institute of Interdisciplinary Studies, Hunan Normal University and Hunan Provincial Key Laboratory for Eco-environmental Changes and Carbon Sequestration of the Dongting Lake Basin, Changsha 410081, China;*
[3] *College of Environmental Science and Engineering, Hunan University and Key Laboratory of Environmental Biology and Pollution Control (Hunan University), Ministry of Education, Changsha 410082, China*

Received September 8, 2023; revised February 8, 2024; accepted February 19, 2024; published online March 28, 2024

Abstract To improve soil carbon sequestration capacity, the full soil carbon cycle process needs to be understood and quantified. It is essential to evaluate whether water erosion acts as a net source or sink of atmospheric CO_2 at the basin scale, which encompasses the entire hydrological process. This study introduced an approach that combined a spatially distributed sediment delivery model and biogeochemical model to estimate the lateral and vertical carbon fluxes by water erosion at the basin scale. Applying this coupling model to the Dongting Lake Basin, the results showed that the annual average amount of soil erosion during 1980–2020 was 1.33×10^{8} t, displaying a decreasing trend followed by a slight increase. Only 12% of the soil organic carbon displacement was ultimately lost in the riverine systems, and the rest was deposited downhill within the basin. The average lateral soil organic carbon loss induced by erosion was 8.86×10^{11} g C in 1980 and 1.50×10^{11} g C in 2020, with a decline rate of 83%. A net land sink for atmospheric CO_2 of 5.54×10^{11} g C a^{-1} occurred during erosion, primarily through sediment burial and dynamic replacement. However, ecological restoration projects and tillage practice policies are still significant in reducing erosion, which could improve the capacity of the carbon sink for recovery beyond the rate of horizontal carbon removal. Moreover, our model enables the spatial explicit simulation of erosion-induced carbon fluxes using cost-effective and easily accessible input data across large spatial scales and long timeframes. Consequently, it offers a valuable tool for predicting the interactions between carbon dynamics, land use changes, and future climate.

Keywords Water erosion, Sediment transfer, Lateral soil carbon loss, Land-atmosphere CO_2 flux, Dongting Lake Basin

Citation: Wang L, Nie X, Li J, Liu Y, Wang H, Li Y, Li Z. 2024. Erosion-induced recovery CO_2 sink offset the horizontal soil organic carbon removal at the basin scale. Science China Earth Sciences, 67(6): 2019–2033, https://doi.org/10.1007/s11430-023-1275-2

1. Introduction

Enhancing the ability of terrestrial ecosystems to act as carbon sinks is a crucial strategy for slowing down global climate change (Friedlingstein et al., 2022). Traditionally, the estimation of terrestrial ecosystem carbon at the global scale has relied on the residual term of the carbon balance equation (Schimel et al., 2001; Wang J et al., 2020). However, this method is unsuitable for the region scale due to the rapid mixing of CO_2, which cannot be accurately monitored (Piao et al., 2022). Hence, it is essential to quantify each component of the terrestrial carbon cycle and simulate its spatial and temporal distribution. Since the 1990s, extensive research has been carried out to estimate terrestrial carbon sinks at the regional scale, with ecosystem process models

* Corresponding author, Xiaodong NIE (nxd@hunnu.edu.cn), Zhongwu LI (lizw@hnu.edu.cn)

being the most popular and fastest-developing type of method for carbon sink assessment in terrestrial ecosystems (Sitch et al., 2008; Baatz et al., 2021). However, these models tend to make a lot of abstractions and simplifications of ecosystem processes for the sake of model efficiency, resulting in significant uncertainty in the simulation results (Doetterl et al., 2016; Li et al., 2022).

Soil is the largest organic carbon pool and a critical component of terrestrial ecosystems (Lal, 2004). However, there have been great differences in estimating soil organic carbon (SOC) storage over the past few decades. Global SOC storages in 1 m depth were estimated to range from 504 to 3400 Pg C, with a median of 1500 Pg C (Scharlemann et al., 2014; Tifafi et al., 2018). Water erosion is the most active process controlling soil formation and evolution, which can affect the redistribution of carbon between terrestrial, aquatic, and atmospheric ecosystems (Borrelli et al., 2017). Erosion-induced organic carbon dynamic process should not be missing in terrestrial carbon cycle simulations. Soil erosion can affect SOC through lateral replacement and vertical turnover (Doetterl et al., 2016). On the lateral way, erosion redistributes soil particles and organic matter, leading to deposits in the lower parts of the landscape or eventually delivered to aquatic ecosystems (Regnier et al., 2022). On the vertical way, the exposure of deep SOC due to erosion of surface soil and the introduction of labile carbon sources can stimulate the decomposition of SOC at eroded sites (Fontaine et al., 2007; de Nijs and Cammeraat, 2020). In addition, most research agrees that erosion reduces plant productivity by weakening the capacity of soil to hold water and nutrients with feedback to the soil carbon balance (Quinton et al., 2010; Kirkels et al., 2014). During sediment transport, the breakdown of aggregates can enhance soil mineralization, while selective transport and deposition increase SOC burial. At deposited sites, efficiently buried SOC establishes large carbon sinks, but the rate and nature of sedimentation, environmental factors, and the time since burial might influence the amount and stability of buried SOC (van Oost et al., 2012; Chaopricha and Marín-Spiotta, 2014).

Although the interactions between SOC dynamics and erosion are still not completely unraveled (Stallard, 1998; Lal, 2003; van Oost et al., 2007; Lal and Pimentel, 2008), various researchers have attempted to model this complex process. The CENTURY model was one of the earliest to account for organic matter dynamics in soil erosion (Parton et al., 1987). However, it only addressed SOC turnover without considering redistribution. Other models, like the Erosion Deposition Carbon Model (EDCM) and Introductory Carbon Balance Model (ICBM), were also developed based on flat terrain assumptions (Andrén and Kätterer, 1997; Liu et al., 2003). Some studies have attempted to integrate soil turnover models with soil erosion models. van Oost et al. (2005) developed the SPEROS-C model, which incorporated ICBM into the spatial representation of soil redistribution processes (SPEROS). This model was widely used at the field and small basin scale and has recently been modified to adapt it for regional-scale applications (Nadeu et al., 2015; Yue et al., 2016). Borrelli et al. (2016) coupled the Revised Universal Soil Loss Equation (RUSLE) with the CENTURY model to quantify the SOC storage response to water erosion. Zhang et al. (2022) developed the ORCHIDEE-$C_{lateral}$ model, which added lateral carbon transport to the ORCHIDEE model and led to a 4.5% increase in simulated annual net terrestrial carbon uptake over Europe. However, these models still have significant uncertainties due to (i) the generalization of model parameters, such as sediment delivery ratio (SDR) and sediment transport coefficient (K_{TC}) (Yue et al., 2016; Borrelli et al., 2018), (ii) the non-connected grids, which simplified the reception or transmission process of SOC from one gird to another (Teng et al., 2022), and (iii) missing process simulation (Doetterl et al., 2016). A model is needed to ensure data availability on a larger scale while reducing assumptions on soil erosion and deposition dynamics.

Due to an insufficient transfer of knowledge regarding soil erosion and carbon dynamics from smaller to larger scales, existing models at a large temporal and spatial scale present conflicting views on whether the net impact of erosion on carbon cycling acts as a carbon source or sink. To investigate the role of erosion in the carbon cycle, we simulate the spatial characteristics of erosion-induced SOC loss in the Dongting Lake basin from 1980 to 2020. Estimating erosion-induced soil carbon processes at a large basin scale can integrate intricate land use patterns and hydrological processes encompassed within the basin. It could not only link terrestrial and aquatic realms but also facilitate incorporation into ecosystem process models. Our hypothesis is that soil erosion can induce a net terrestrial sink for atmospheric CO_2 at the basin scale. To test this hypothesis, we estimated net soil erosion and deposition rates by combining the Chinese soil loss equation (CSLE) with the transport-limited sediment delivery (TLSD) model. The lateral loss of SOC detached by water erosion was calculated on its founders. The vertical CO_2 fluxes during the erosion process were also quantified by a modified ICBM model. This coupling model holds the potential to quantify the essential role of human activities, including ecological projects and economic construction, to estimate the size of regional land carbon sinks and mitigate climate change.

2. Model development and evaluation

2.1 Study area

The Dongting Lake Basin is located in the center of the Yangtze River basin (24.64°N–30.41°N, 107.28°E–114.25°

E), covering approximately 2.67×10^5 km^2 (Figure 1). The Dongting Lake receives water predominantly from the Yangtze River and four upstream tributaries (Xiang River, Zi River, Yuan River, and Li River) and discharges into the Yangtze River through a northern outlet. Correspondingly, the basin can be divided into four river sub-basins and the Dongting Lake Plain. The Dongting Lake basin is characterized by a subtropical monsoon climate with a mean annual temperature of 16–19°C and a mean annual precipitation of 1200–1400 mm. The basin has complex topography sloping from the south to the center and northeast with hills, low mountainous, and plains. According to the Chinese Soil Taxonomy, soil in the Dongting Lake Basin can be classified into six orders, namely Anthrosols, Cambosols, Argosols, Ferrosols, Primosols, and Gleysols, more than one-third of which are Ferrosols. The predominant land use types in the basin are forest (hardwoods, conifers, and mixed) and farmland (rice, vegetation, and rapeseed). Due to its strong spatial heterogeneity of climate, terrain, soil, and vegetation, SOC storage and erosion intensity exhibit significant spatial variability, resulting in different SOC dynamic processes in different regions. Over the past 20 years, large-scale ecological restoration projects have successfully reduced soil erosion intensity in most areas of the basin (Wang et al., 2021; Wang L et al., 2022). Conversely, extreme climatic events and cropland and cash forest construction have led to increased soil erosion intensity in a few areas.

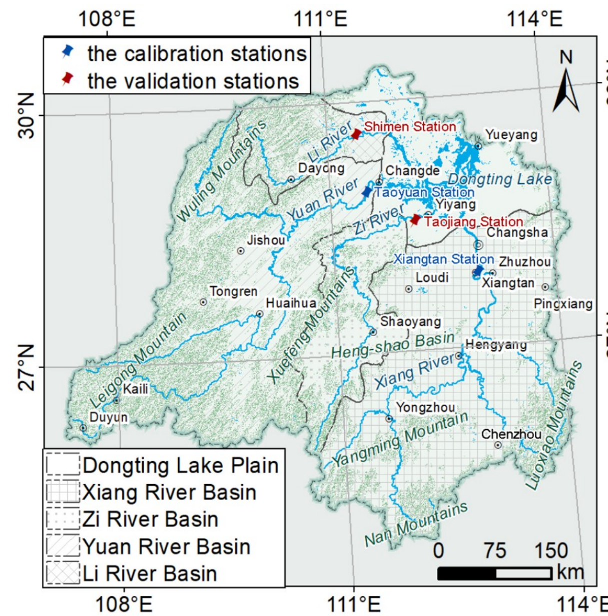

Figure 1 Map of the study shows the terrain, river system, and sediment monitoring station.

2.2 Soil loss and sediment transfer

The CSLE and TLSD models were selected to model the three sub-processes of the soil erosion process, namely soil loss, sediment transport, and sediment deposition (Jain and Das, 2009; Lin et al., 2020). Based on USLE, the CSLE model was proposed to reflect the terrain features and soil conservation measures in China (Duan et al., 2020). The TLSD model adopted a grid-based procedure for the discretization of the basin. The eroded sediment from each cell follows a specific route formed by the topography and finally sinks at the outlet of the basin. This method is suitable for complex landscapes with gullies and hills, like the Dongting Lake basin, to estimate net fluxes of erosion and deposition (Verstraeten et al., 2007). The simulation equations of the three sub-processes of the soil erosion process are as follows.

(i) Sub-process 1. Soil erosion

The soil erosion is estimated by the CSLE (eq. (1)),

$$\mathrm{SE} = R \times K \times L \times S_{\mathrm{2D}} \times B \times E \times T, \tag{1}$$

where SE is the soil erosion modulus (t ha^{-1}a^{-1}); R is the rainfall intensity factor (MJ mm ha^{-1} h^{-1} a^{-1}); K is the soil erodibility factor (t ha h ha^{-1} MJ^{-1} mm^{-1}); L and S_{2D} are the two-dimensional slope length and steepness factors, respectively; B, E, and T are the dimensionless factors of biomass-control, engineering-control, and tillage practices, respectively. The estimation method of parameterization of the CSLE model can be referred to Wang L et al. (2020) (Appendix S1, https://link.springer.com/). We used the Mann-Kendall (MK) test to analyze annual soil erosion trends from 1980 to 2020. The MK test is non-parametric, meaning it does not assume a specific distribution for the observed data and is particularly suitable for non-normally distributed data.

(ii) Sub-process 2. Sediment transport

The Sediment transport capacity was calculated by the equation proposed by Verstraeten et al. (2007).

$$\mathrm{TC} = K_{\mathrm{TC}} \times R \times K \times A_{\mathrm{s}}^{1.44} \times S_{\mathrm{3D}}^{1.44}, \tag{2}$$

where TC is the sediment transport capacity (t ha^{-1}a^{-1}); K_{TC} is the transport capacity coefficient depending on land use and cover types (dimensionless); A_{s} is the specific catchment area contributed by the upslope per unit contour length (hm^2 hm^{-1}); S_{3D} is the local slope for three-dimensional landscapes (hm hm^{-1}). The spatial pattern of K_{TC} was estimated by the exponential function of NDVI (eq. (3)) (Jain and Das, 2009),

$$K_{\mathrm{TC}} = \beta \times \exp\left(\frac{-\mathrm{NDVI}}{1-\mathrm{NDVI}}\right), \tag{3}$$

where β is the calibration coefficient, which is used to adjust the error between the observed and predicted sediment yield.

(iii) Sub-process 3. Sediment deposition

$$T_{\mathrm{out}} = \min\left(\mathrm{SE} + \sum T_{\mathrm{in}}, \mathrm{TC}\right), \tag{4}$$

$$\mathrm{SD} = \mathrm{SE} + \sum T_{\mathrm{in}} - T_{\mathrm{out}}, \tag{5}$$

where T_{in} is the sediment inflow in the current cell from upstream cells; T_{out} is the sediment outflow from the current cell; SD is sediment deposition modulus in the current cell (t ha^{-1}a^{-1}). The net erosion map is calculated as the difference between the soil erosion modulus and deposition modulus for each grid cell. Positive values on the net erosion map are net erosion modulus (netSE, t ha^{-1}a^{-1}), whereas negative values represent net deposition modulus (netSD, t ha^{-1}a^{-1}).

2.3 Lateral and vertical carbon fluxes

Yue et al. (2016) proposed a modified model to assess erosion-induced SOC fluxes at a large scale based on the study of van Oost et al. (2007) and successfully applied it in China. However, this model used the SDR to model sediment supply, which did not consider the spatial variability of sediment delivery and deposition. Therefore, the gird cells simulated carbon fluxes were actually non-connected units, which could not reflect the inflow and outflow of SOC from one to another. Here, we used the TLSD model to further modify this model to predict SOC delivery to bridge the gap (Figure 2 and Figure S1).

(i) Lateral carbon fluxes (F_L)

$$F_L = \mathrm{SOCC}_{top} \times (\mathrm{SE} - \mathrm{SD}) \times A, \quad (6)$$

where F_L is the total amount of lateral carbon induced by erosion (kg a^{-1}); SOCC_{top} is the SOC content (g kg^{-1}) in the topsoil, which dominates erosion; A is the current cell area (ha).

(ii) Vertical carbon fluxes (F_V)

$$F_V = F_{V\text{-}E} + F_{V\text{-}T} + F_{V\text{-}D}, \quad (7)$$

where F_V is the total amount of vertical carbon induced by erosion (g a^{-1}); $F_{V\text{-}E}$, $F_{V\text{-}T}$, and $F_{V\text{-}D}$ are the components of F_V during erosion, transport, and deposition, respectively.

$$F_{V\text{-}E} = (C - C_e) \times A, \quad (8)$$

where C is carbon fluxes without the impact of erosion (g m^{-2} a^{-1}); C_e is carbon fluxes with the impact of erosion (g m^{-2} a^{-1}). The differential equations describing the carbon flux dynamics are:

$$\frac{dC}{dt} = I - K_O \times C, \quad (9)$$

$$\frac{dC_e}{dt} = I - (K_O + K_E) \times C_e + \mathrm{SOCC}_{bottom} \times \mathrm{netSE}, \quad (10)$$

where I is the carbon input to the soil, which was assumed to be equal to the net primary production (NPP, g m^{-2} a^{-1}); K_O is the turnover rate of SOC with respect to decomposition without erosion; K_E is the erosion rate of SOC, which can be calculated by dividing the ratio of soil erosion rate by the depth of carbon in top soil layer; SOCC_{bottom} is the SOC content (g kg^{-1}) at the bottom of the top soil layer.

$F_{V\text{-}T}$ is the F_V during sediment transport, which was assumed to be 63% of the *in-situ* organic carbon decomposition, referring to Yue et al. (2016) and Guenet et al. (2013)

$$F_{V\text{-}T} = 0.63 \times \mathrm{SOCC}_{top} \times \mathrm{netSE} \times K_O \times A, \quad (11)$$

$$F_{V\text{-}D} = \mathrm{SOCC}_{top} \times \mathrm{netSD} \times K_{O\text{-}s} \times A, \quad (12)$$

where $K_{O\text{-}s}$ is the turnover rate of the subsoil layer.

2.4 Model parameterization and calibration

The model was implemented using ArcGIS10.6 and the Terrain Analysis Using Digital Elevation Models (TauDEM) on the basis of the remote sensing image of the Dongting Lake Basin. Table 1 summarizes the input data required for the model and its description and source. Since the hydrologic information driving sediment transportation is calculated based on the digital elevation model (DEM), all space parameters were resampled to the spatial resolution of DEM

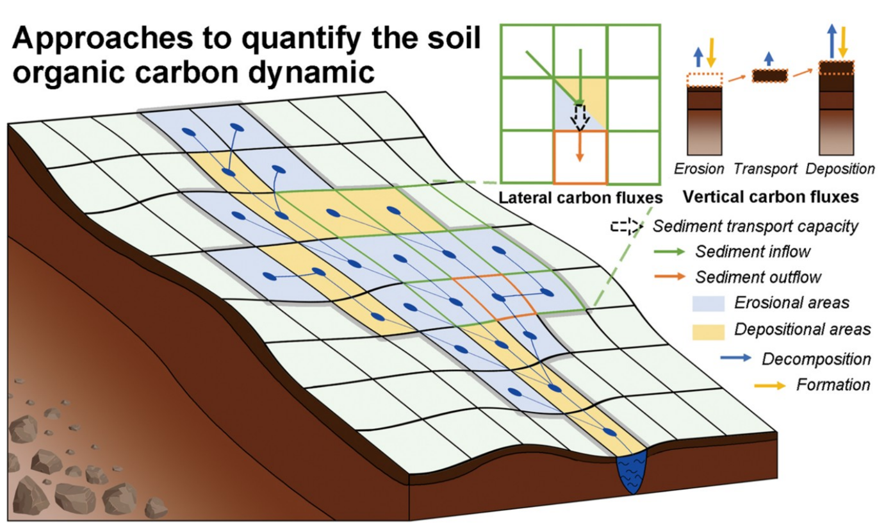

Figure 2 Schematic showing discretized grid cells and all soil organic carbon fluxes in the basin.

Table 1 Summary of input data required for the model[a)]

Input data	Spatial resolution	Temporal resolution	Source year	Data source	Equation
MAT, MAP	P	D: daily	1980–2020	120 meteorological stations	(1), (2)
DEM	G: 30 m	S	2000–2009	ASTER GDEM.	(1), (2)
LUC	G: 30 m	D: yearly	1980–2020	China Multi-Period Land Use Land Cover Remote Sensing Monitoring Data Set (Xu et al., 2018)	(1)
K	G: 30 m	S	2018	Grid Data on Soil Erodibility in China (Liu et al., 2018)	(1), (2)
SOCC	P	S: 2 years	1980s, 2010s	The three-dimensional spatial distribution of SOC (Appendix S2)	(6), (8)–(12)
NDVI	G: 250m	D: yearly or 16 days	1980–2020	Global GIMMS NDVI3g v1 dataset and MOD13Q1 data	(1), (3)
NPP	G: 0.0727°	D: yearly	1981–2019	The dataset of simulated daily net primary productivity over the globe.	(9), (10)
Rs	G: 1000 m	S	2020	The global annual mean soil respiration product (Huang et al., 2020).	(9), (10)

a) MAT, mean annual temperature; MAP, mean annual precipitation; LUC, land use and land cover; *K*, soil erodibility factor; SOCC, soil organic carbon content; NDVI, normalized difference vegetation index; NPP, net primary production; Rs, soil respiration; Spatial resolution: raster (G), station or profile (P); Temporal resolution: static (S), interval (D)

(30 m) through the nearest neighbor method (discrete data, such as land use) and the bilinear interpolation method (continuous data, such as soil respiration).

In this study, the observed annual sediment discharges, which were collected from the Xiangtan hydrological station (Xiang River Basin), Taojiang hydrological station (Zi River Basin), Taoyuan hydrological station (Yuan River Basin), and Shimen hydrological station (Li River Basin) from1980 to 2020, were used to calibrate and validation the parameter β within the CSLE-TLSD model. The Nash coefficient was calculated to evaluate the accuracy of the model (Nash and Sutcliffe, 1970),

$$\mathrm{NSE} = 1 - \frac{\sum_{i=1}^{n}(O_i - P_i)^2}{\sum_{i=1}^{n}\left(O_i - \overline{O}\right)^2}, \tag{13}$$

where n is the observation frequency of sediment yield; O_i and P_i are observed and estimated sediment yields, respectively; $\overline{O}$ is an average value of observed sediment yields. NSE∈[−∞, 1]. The efficiency of the model emulation increases as *NSE* moves more in that direction.

3. Results

3.1 Model calibration

To calibrate the parameter β and assess model performance, simulation results were compared with annual sediment yield data observed at hydrological stations in four sub-basins from 1980 to 2020. The observation data from Xiangtan and Taoyuan stations were randomly selected to calibrate parameters, while the observation data from Taojiang and Shimen stations were used for model evaluation. The model was looped 10 times with the β parameter, which was set between 0.05 and 0.15 with an interval of 0.01, to select the best model with the highest NSE. When the calibration coefficient β is 0.1, the NSE of the model was the highest at 0.38. Under this condition, the simulated and observed annual sediment yields at the validation stations agreed well (NSE=0.36). While the observed and simulated values of Yuan River Basin and Zi River Basin displayed good linear fitting (R^2>0.6), those of Li River Basin and Xiang River Basin showed underfitting (Figure 3). This is likely due to river management practices, particularly reservoir trapping, leading to lateral sediment flows from land to rivers that are not strictly consistent with the observation data from hydrological stations. In the Xiang River basin, there are as many as 51 dams (Wang X et al., 2022), which is substantially higher than other sub-basins, thereby reducing the accuracy of verification using the observation data of the hydrology station. In addition, a heavy rainstorm occurred in the Li River Basin in 1980, resulting in the highest sediment yield over the past 50 years. However, the CSLE model struggled to identify this anomaly, leading to the reduced prediction accuracy of the Li River Basin. Although the model may not exhibit high predictive accuracy for certain sub-basins or specific years, it still can reflect spatiotemporal heterogeneity of soil erosion in the whole basin.

3.2 Soil erosion

The annual average soil erosion modulus during 1980–2020

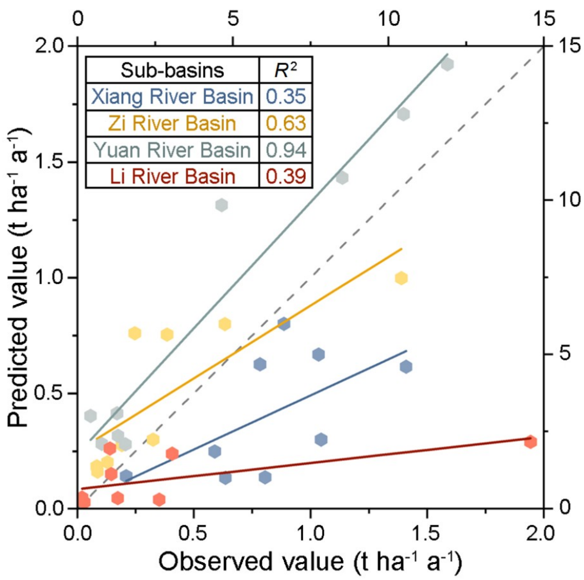

Figure 3 Performance of the CSLE-TLSD model predicting sediment yield in four sub-basins when β=0.1. The simulated and observed sediment yields of the Li River Basin were represented on the top and right axes, while the remaining sub-basins were represented on the bottom and left axes.

in Dongting Lake Basin was 5.09 t ha^{-1} a^{-1} (Figure 4a). Areas classified as having no apparent erosion (Soil erosion modulus<1 t ha^{-1} a^{-1}) were about 65% of the total basin area. The areas classified as having erosion in Dongting Lake Plain were only 16% of the sub-basin area. The erosion modulus showed an east-west oriented increasing gradient. The land with exceeding the generic tolerable soil loss (Soil erosion modulus >10 t ha^{-1} a^{-1}) was distributed in northwestern, western, and southern hilly areas of the basin.

The soil erosion amount in Dongting Lake Basin showed an overall decreasing trend during 1980–2020, with the highest in 1980 at 2.00×10^8 t a^{-1} and the lowest in 2005 at 0.97×10^8 t a^{-1} (Figure 4b). It was noteworthy that the small increase in erosion amount during 2005–2015 was not accompanied by an increase in apparently eroded areas. It indicated a trend of further deterioration in areas where erosion was already severe. From the MK test (Figure 4c), a spatially heterogeneous mixture of positive and negative change trends of soil erosion modulus was found, and the primary trend was negative. Areas suffering significant erosion increment were mainly found in regions around Dongting Lake or cities with rapid economic development.

Eroded districts (SE>SD) accounted for 55% of the total basin area, while 24% of land was a depositional district (SE<SD). The positive value of the difference between potential erosion and deposition is the net erosion, which represents the actual amount of soil leaving the landscape and entering the rivers. The sum of the net erosion of the basin is the sediment yield. The average sediment yield predicted by the model for Dongting Lake Basin totals 1.56×10^7 t a^{-1} during 40 years. The SDR was about 0.12, which is in good agreement with the estimated results of Li et al. (1995).

3.3 Erosion-induced lateral carbon fluxes

This study investigates the erosion-induced F_L in Dongting Lake during the last 40 years (Table 2 andTable S1). The F_L is indicative of both the net loss of organic carbon into the riverine system (F_L>0) and the net redeposition of organic carbon across the landscape (F_L<0). Results indicated that 8.86×10^{11} g C would be lost in the riverine system in 1980, accounting for 17.6% of the SOC displacement. While the loss had fallen to 1.50×10^{11} g C in 2020, accounting for only 4.5% of the SOC displacement. Previous studies also reported that 50%–95% of the eroded material would finally deposit downhill (Stallard, 1998; Ran et al., 2014; Panagos et al., 2015; Dialynas et al., 2016). The average F_L of the Li River Basin and the Yuan River Basin, both of which had initial intensive erosion and high SOC content, were much higher than that of other sub-basins (Figure S2a and S2b). The lowest average F_L of 0.63 g C m^{-2} a^{-1} was observed in the Dongting Lake Plain.

From 1980 to 2020, the total carbon flowing into the river decreased by 7.35×10^{11} g C in Dongting Lake Basin. Among the sub-basins, the total amount of SOC loss decreased the most in the Yuan River Basin, while the decline rate of SOC loss was highest in the Li River Basin. The total amount of net erosion decreased and SOC content increased in these basins. The areas with reduced F_L accounted for 60% of the entire basin area, while the areas with increased F_L accounted for 20% (Figure S3). Within the regions where F_L increased, 68% were depositional districts. The reduction in F_L within these districts was primarily attributed to a decrease in netSD, while any impact resulting from changes in SOC was not readily apparent. Conversely, within erosion areas, the trends observed for netSE and SOC changes were predominantly opposite. Combining these two factors ultimately resulted in an overall increase in F_L.

Regarding all land use types in the Dongting Lake Basin (Figure 5), grassland experienced the largest erosion-induced F_L (average F_L of 8.70 g C m^{-2}, and total loss of 1.30×10^{11} g), followed by cropland (average F_L of 1.98 g C m^{-2}, and total loss of 1.47×10^{11} g) and forest (average F_L of 1.53 g C m^{-2}, and total loss of 2.42×10^{11} g). Except for the unutilized land, the deposition area proportion of other land use types increased from 1980 to 2020, especially forest and grassland. The erosion area proportion of construction land increased significantly, while other land used types decreased. Only the F_L of construction land exhibited an upward trend, while the corresponding expansion of the construction land area resulted in a simultaneous increase in organic carbon discharge into rivers. Specifically, over 40 years, the organic carbon input from construction

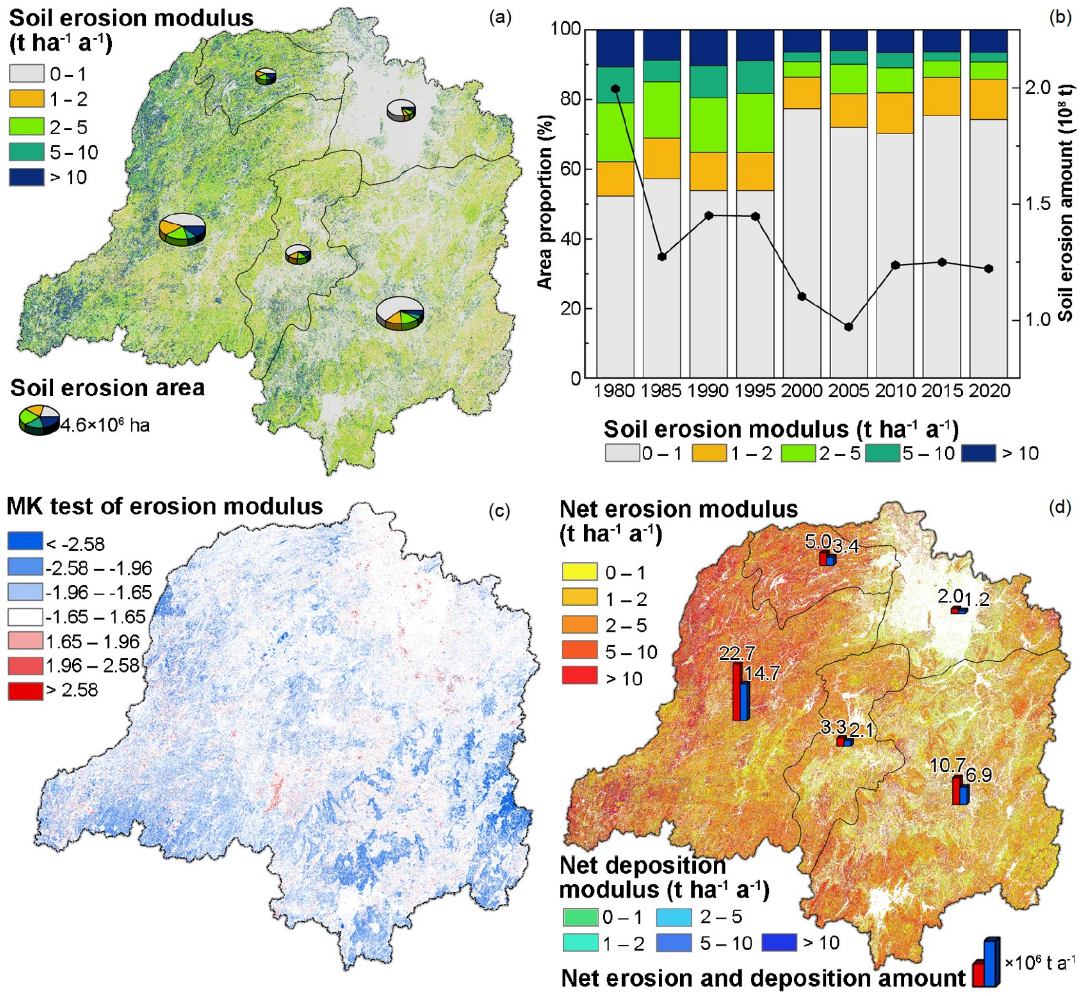

Figure 4 Estimated annual average soil loss and deposition rate for Dongting Lake Basin based on CSLE-TLSD model. (a) Annual average soil erosion modulus; (b) change of area proportion of soil erosion class and soil erosion amount during 1980–2020; (c) spatial pattern of MK test significance of soil erosion modulus; (d) annual average net soil erosion modulus and deposition modulus.

Table 2 The erosion-induced lateral carbon fluxes for each sub-basin from 1980 to 2020

Sub-basin	Mean F_L (g C m^{-2})			Total loss (10^{10} g C)			Decline rate
	1980	2020	2020–1980	1980	2020	2020–1980	
Dongting Lake Plain	0.88	0.38	−0.51	2.56	1.04	−1.52	59.5%
Xiang River Basin	1.47	0.36	−1.11	13.59	3.27	−10.32	76.0%
Zi River Basin	1.91	0.5	−1.41	4.86	1.27	−3.59	73.8%
Yuan River Basin	6.01	0.85	−5.16	53.64	7.53	−46.12	86.0%
Li River Basin	7.86	1.09	−6.77	13.9	1.91	−11.99	86.3%
Dongting Lake Basin	3.49	0.6	−2.89	88.55	15.01	−73.54	83.0%

land amplified by 2.76×10^8 g.

3.4 Erosion-induced vertical carbon fluxes

Soil erosion consists of three phases: detachment, transport, and deposition. Hence, this study conducted a simulation of the impacts of erosion on land-atmosphere CO_2 fluxes in three parts, namely, eroded district, depositional district, and transport process (Table 3).

The eroded carbon is replaced through photosynthetic processes to achieve a new carbon cycle balance and finally a net atmospheric carbon sink. Harden et al. (1999) first coined this phenomenon as ‘dynamic replacement’. To estimate erosional loss and concomitant replacement of organic car-

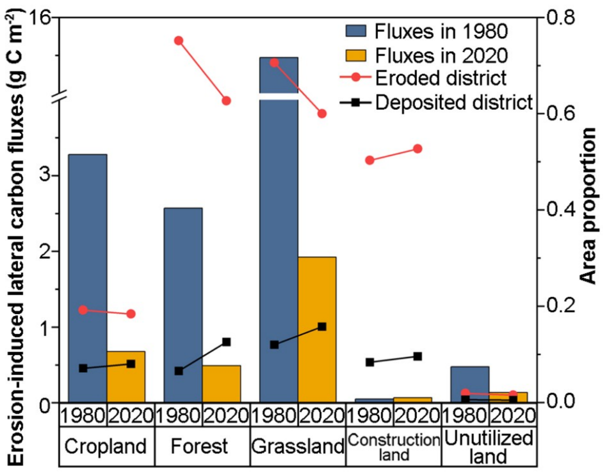

Figure 5 The erosion-induced lateral carbon fluxes in different land use types and its area proportion of eroded districts (potential erosion amount > potential deposition amount) and deposited districts (potential erosion amount < potential deposition amount).

bon at eroded district, a model with a zero-order carbon accumulation and first-order carbon loss was constructed and modified based on the research of Yue et al. (2016), van Oost et al. (2007), and Stallard (1998). This method simulates the processes of SOC composition/decomposition and lateral movement, respectively, based on the assumption that erosion did not impact the original CO_2 exchange process. The difference in carbon storage with or without the impact of erosion on CO_2 emission/sequestration under the two conditions is considered as the erosion-induced CO_2 flux in the eroded district. We modified this method by excluding simple SDR obtained from regression analysis and replacing it with the net erosion and deposition modulus. The results showed that the CO_2 uptake in the eroded district was 9.43×10^{11} g C in 1980 and 3.33×10^{11} g C in 2020, decreasing by 64.71%. Spatial distributions of regions with high F_L and F_V were similar (Figure 6 and Figure S4). Severely eroded areas in the Yuan River Basin significantly contributed to the recovery CO_2 sink. Table 3 shows that the erosion-induced carbon sink contributed by Li River Basin is two times that of Zi River Basin, although the erosion areas of these two sub-basins are similar. This discovery aligned with the view of Stewart et al. (2007) that soils further from carbon saturation might experience the highest level of efficiency in SOC sequestration.

During sediment transport, the breakdown of aggregates leads to an increase in organic carbon mineralization. This is because the intra-aggregate pores are the preferred sites of sorption for SOC. Hence, this easily mineralizable carbon gets quickly released into the atmosphere upon the breakdown of aggregates (Ananyeva et al., 2013). Yue et al. (2016) relied on the microcosm experiment conducted by Guenet et al. (2013) and utilized 63% relative to the fluxes of the reference source soil to represent the CO_2 flux induced by erosion during sediment transport. We adopted this method and found that the flux component in the transport process resulted in a CO_2 source of 9.83×10^{10} g C in 1980 and 1.26×10^{10} g C in 2020, indicating a decline of 8.57×10^{10} g C. However, Doetterl et al. (2016) have pointed out that increased mineralization differs significantly during the transport process, ranging from 0% to 100% of the *in-situ* organic carbon decomposition, which might be influenced by rain intensity and land cover. Given the limited theoretical understanding and data availability, a relatively median and widely used coefficient of 0.63 was used to estimate the CO_2 flux during sediment transport. The results only reflect the general change trend, and their quantity may not be completely accurate. Despite this, the CO_2 release induced by erosion during the transport process is relatively small compared to the CO_2 uptake caused by erosion in the eroded district. Therefore, the uncertainty associated with this component would not significantly affect the overall results of vertical flux.

The decomposition of newly buried carbon-rich soil and the resulting emission of additional CO_2 into the atmosphere within the depositional district can diminish the effectiveness of the soil carbon sink (Hoffmann et al., 2013). Assuming minimal changes to the deposited soil during transport, it can have a similar concentration as the previous topsoil. Generally, the subsoil layer has a slower carbon turnover rate compared to the topsoil (Schmidt et al., 2011). The buried soil with an equivalent amount as the net deposited soil

Table 3 The erosion-induced vertical carbon fluxes for each sub-basin from 1980 to 2020

Sub-basins	F_{V-E} (10^{10} g)		F_{V-T} (10^9 g)		F_{V-D} (10^9 g)		F_V (10^{10} g)		
	1980	2020	1980	2020	1980	2020	1980	2020	2020–1980
Dongting Lake Plain	2.23	1.74	3.43	0.80	1.71	0.36	1.72	1.63	−0.09
Xiang River Basin	16.67	6.48	18.14	3.24	9.62	1.68	13.89	5.98	−7.91
Zi River Basin	7.20	2.55	5.82	1.06	3.08	0.51	6.31	2.40	−3.92
Yuan River Basin	51.76	17.99	56.94	5.85	29.48	2.88	43.12	17.11	−26.00
Li River Basin	16.41	4.51	13.97	1.59	7.51	0.84	14.27	4.27	−10.00
Dongting Lake Basin	94.28	33.27	98.29	12.55	51.40	6.27	79.31	31.39	−47.92

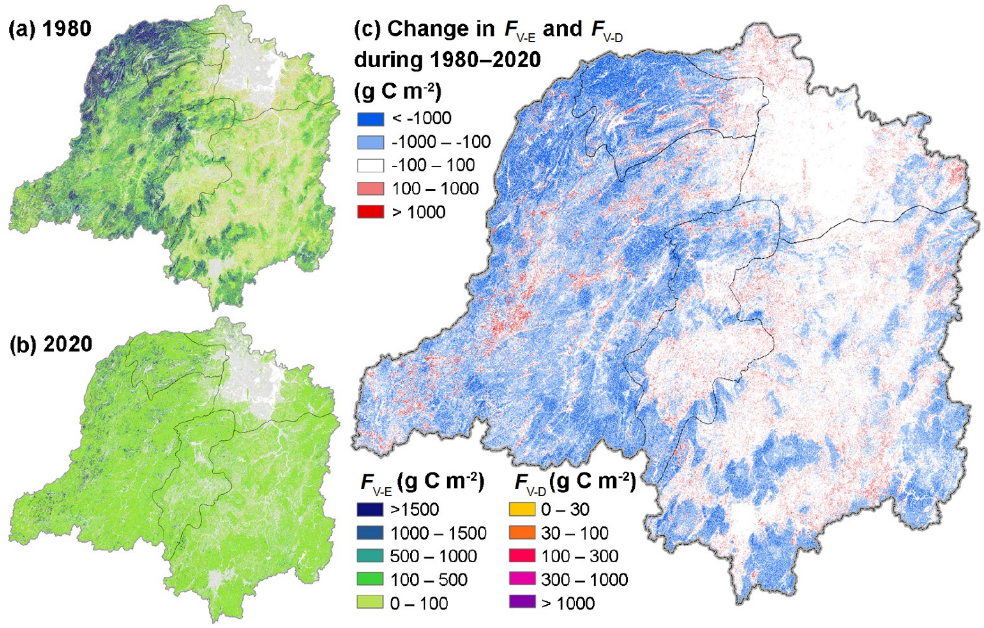

Figure 6 The spatial pattern of erosion-induced vertical carbon fluxes in the eroded district ($F_{V\text{-}E}$) and depositional district ($F_{V\text{-}D}$). (a) 1980; (b) 2020; (c) its change during 40 years.

mineralized at the turnover rate of deep SOC is the newly added F_V in the depositional district. In 1980, this flux component was 2.87 g m^{-2}, while it decreased to 0.2 g m^{-2} over four decades, indicating a decline of 4.51×10^{10} g C. Although the area of the CO_2 source decreased and increased due to erosion almost equally in the depositional district, the decrease rate was 30 times faster than the increase rate. However, more easily decomposable carbon fractions of buried soil might significantly degrade during sediment transport, deposition, and burial in reality. The FVD in this study might be overestimated. Our hypothesis is acceptable for short timescales, but the rate of soil burial, the amount and nature of mobilized carbon, and environmental conditions jointly influence the amount of buried carbon as time passes (Doetterl et al., 2016). When the time scale is extended to the centennial scale, environmental conditions become the dominant factor (van Oost et al., 2012).

4. Discussion

4.1 Soil organic carbon dynamics in eroding landscapes

This study examines the carbon loss caused by erosion using an integrated sediment delivery-biogeochemical model that integrates various datasets. The annual average lateral SOC loss modulus at the topsoil was evaluated as 2.05 g C m^{-2}. Yue et al. (2016) reported it was 7.44 g C m^{-2} in central China and 24.51 g C m^{-2} in Southwest China. These two regions contained part of the Dongting Lake Basin and had higher lateral SOC loss induced by erosion than our study. This might be because the different sources of SOC maps were used to model carbon erosion. Yue et al. (2016) used the Global Soil Dataset with a resolution of 1 km, which might underestimate the actual values and ignore the interannual variation of SOC. Moreover, the SDRs, which were used in the erosion model of Yue et al. (2016), increased the uncertainty of the results. Yang et al. (2020) estimated that the redistribution rate of SOC caused by erosion was 2.1 g C m^{-2} in the midstream of the Yangtze River Basin from 1992 to 2013, which agreed well with our study.

The annual average erosion-induced vertical SOC sink modulus at the topsoil was evaluated as 5.54×10^{10} g in this study. Dialynas et al. (2016) conducted a study on the Mameyes and Icacos basins and reported that the basin-integrated carbon exchange with the atmosphere ranged from −18.3–+21.5 g m^{-2} and −14.9–+17.1 g m^{-2} (−, carbon sources; +, carbon sinks), respectively. This work stressed the role of erosion in the carbon cycle depending on the forest type and land use. Izaurralde et al. (2007) compared the soil carbon balance in three basins with different management practices and found that the conventional till continuous basin acted as a carbon source for atmospheric CO_2, while the no-till system basins were sinks of carbon to the atmosphere. In the studies above, different scenarios were set up, which were directly related to anthropogenic disturbances, such as agricultural practices. In this study, the organic carbon lost to riverine systems exceeded the recovery CO_2 sink in 1980, but this trend was reversed by 2020. Yue et al. (2016) also confirmed this rising trend of erosion-induced carbon sink in the Southeast region of China. It implied an increasing trend of soil carbon retention capacity in the

Dongting Lake Basin during the 40 years.

It is widely accepted that the allocation and management of land use determines whether erosion will act as a source or sink of atmospheric carbon (Lal, 2004). Over the past 40 years, the Grain for Green Project has been one of the most critical ecological restoration projects in the Dongting Lake Basin. This project has demonstrated substantial synergistic benefits in carbon sequestration by enhancing plant growth, carbon input to soils, and reducing lateral carbon replacement and decomposition during sediment transport (Zeng et al., 2020; Wang L et al., 2022). Without land use type change, most land management practices with less anthropogenic disturbance can also improve SOC accumulation. Forest and cultivated land are the primary land use types where management policies are implemented in Dongting Lake Basin. The adoption of no-tillage farming practices can effectively reduce SOC redistribution and surficial SOC loss, thereby reducing the impact of erosion on the carbon cycle (Izaurralde et al., 2007; Amelung et al., 2020; Kwang et al., 2023). SOC storage in forests, on the other hand, is more susceptible to CO_2 emissions from sources such as forest fires, biomass burning, and rotational farming, and the reduction of organic matter input due to removing litter, harvesting, and applying lime fertilizer (Ramesh et al., 2019). These examples collectively highlight the negative impact of anthropogenic disturbance on SOC storage. In the short term, implementing hillside closure for erosion control can enhance soil carbon storage. However, it is essential to note that undisturbed mature forests eventually reach a state of relative carbon balance (fixation rate=decomposition rate), limiting the long-term sustainability of this effect (Jiang et al., 2020). Therefore, identifying appropriate land use strategies and effective management practices is paramount in mitigating climate change through enhanced carbon sequestration in soil.

4.2 Process-oriented modeling of carbon redistribution

A well-designed model for SOC redistribution should effectively address the spatial and temporal discrepancies between local processes with short-term and long-term effects at the landscape scale. Several process-oriented water erosion models have been developed. Specifically, Doetterl et al. (2016) reported eight coupled soil erosion and SOC turnover models, mainly applied at soil profiles and local scales. However, recently developed models have expanded their application to much larger scales and have sought to integrate with existing Earth System Models (ESM). For instance, Tan et al. (2020) coupled a newly developed event-based soil erosion model with the US Department of Energy's Energy Exascale ESM to estimate the impact of soil erosion on carbon cycling over the continental United States. Additionally, Zhang et al. (2022) incorporated the fluvial transfer of sediment and organic carbon into the ORCHIDEE land surface model. While at the local scale, more recent models have been predominantly used to predict SOC dynamics across a large variety of settings and scenarios, such as erosion intensity, climate conditions, or tillage practices (Nadeu et al., 2015; Dialynas et al., 2016). We updated the overview of coupled soil erosion and SOC turnover models (Table 4). Most models coupling erosion to SOC turnover are predominantly based on the Universal Soil Loss Equation (USLE) family models and the SPEROS-C model. These models were designed in an annual time step, making collecting input spatial data at large scales easy. Furthermore, existing models are gradually taking more carbon processes into account. For example, whereas previous models usually solely focused on particulate organic carbon (POC) fluxes, Zhang et al. (2022) took leaching of soil dissolved organic carbon (DOC) into their model, resulting in promising advancements in estimating carbon cycling in dynamic landscapes. Nevertheless, as computing power and data availability improve, it is still necessary to constantly refine the carbon dynamic process and enhance the generalization of model parameters.

Since the basin is the basic hydrologic unit, systematically simulating water erosion-induced carbon fluxes at the basin scale is a key link for simulating the terrestrial ecosystem carbon cycle. The expression of the erosion process varies across different scale models. Due to limitations in the availability of input data and the requirements of computing power, a bottom-up series of models is necessary to isolate key environmental factors affecting SOC. Specifically, the models at the micro-scale (particle, aggregate, and pedon) are employed to investigate crucial physical, geochemical, and biochemical mechanisms underlying carbon stabilization. These findings can be extrapolated to the basin scale to enhance our incomplete comprehension of carbon dynamic processes. The models at the global scale provide a stronger connection between carbon sequestration schemes and climate change policies but with notable uncertainty. To improve the accuracy of SOC estimation at the global scale, further development of large basin-scale models is still needed to ultimately elucidate the interconnections between lateral soil fluxes and terrestrial-aquatic carbon cycling.

Our method replaced the simple SDR with a sediment dynamics model and estimated the continuous three-dimensional spatial distribution of initial SOC, both of which provided a better description of the spatial heterogeneity of carbon dynamics induced by erosion. Although we focused our analysis and modeling on the Dongting Lake Basin because of the data availability and our work foundation, this model could be applicable to the rest of the world because the Dongting Lake Basin already represents a key influence of soil erosion in recent years, like extreme climatic, diverse land management, and ecological restoration projects. According to Table 4, the application of SOC simulation

Table 4 Summary of modeling C dynamics in eroding landscapes at different scales

Scale	Extent			Area (km^2)	Timescale	Scenario	Carbon fluxes ($g\ m^{-2}$)		Model	References
							Lateral	Vertical		
Global	Global			1.49×10^8	/	Current	33.56	6.71	/	Lal, 2003
Regional	China			9.60×10^6	1995–1996	Current	11.98	5.25	modified SPEROS-C	Yue et al., 2016
					2010–2012		5.29	4.25		
	European agricultural soils			1.87×10^6	2000–2010	Current	1.50	0.70	CENTURY +USLE	Lugato et al., 2016
	Australia			7.69×10^6	1950s–1990	Current	0.53	0.21	/	Chappell et al., 2014
	United States of America			7.42×10^6	1991–2012	Current	1.89	/	ELM-Erosion	Tan et al., 2020
	China	the Tibetan Plateau		2.50×10^6	2001–2017	Current	0.96	/	RUSLE	Teng et al., 2022
	China	the Yellow River Basin		7.95×10^5	1950–2010	Current	22.43	6.06	/	Ran et al., 2014
	China	the Yellow River Basin		7.95×10^5	1992–2013	Current	3.8	/	USPED	Yang et al., 2020
		the Yangtze River Basin		1.80×10^6			4.2	/		
		the Pearl River Basin		4.42×10^5			2.9	/		
	Europe	the Rhine catchment		1.85×10^5	1851–1861	Current	0.0012	0.32	CE-DYNAM	Naipal et al., 2020
					1995–2005		0.0009	0.73		
	Europe and parts of the Middle East			1.51×10^7	1901–2014	Current	3.14	3.78	ORCHIDEE-Clateral	Zhang et al., 2022
Local	the central Belgium			2.50×10^2	/	conventional tillage	2.30	2.70	SPEROS-C	Nadeu et al., 2015
						reduced tillage	2.30	2.50		
						reduced tillage with additional carbon input	1.20	11.20		
	Puerto Rico	the Mameyes watershed		17.8	/	maximum source	14.90	−18.30	tRIBS-ECO	Dialynas et al., 2016
						intermediate	25.30	6.00		
						maximum sink	39.20	21.50		
		the Icacos watershed		3.26		maximum source	32.40	−14.90		
						intermediate	40.10	3.30		
						maximum sink	52.10	17.10		
	Germany	the arable catchment 1		3.70×10^{-2}	1994–2001	Current	0.31	0.26	MCST-C	Wilken et al., 2017
		the arable catchment 2		7.80×10^{-2}			0.13	0.58		
	Germany	the Heiderhof test site		4.20×10^{-2}	1950–2007	Current	7.70	0.90	SPEROS-C	Dlugoß et al., 2012
	United States of America		the Nelson Farm	2.09×10^{-2}	1870–1997	minimum erosion	19.16	−13.00	EDCM	Liu et al., 2003
						maximum erosion	34.40	−24.00		
	United States of America	the North Appalachian Experimental Watershed	W118	7.90×10^{-3}	1951–1999	corn-soybean no-till rotation	0.39	5.51	EPIC+USLE	Izaurralde et al., 2007
			W128	1.08×10^{-2}	1966–2001	conventional till continuous corn	0.82	−1.03		
			W188	8.30×10^{-3}	1966–2001	under no-till continuous corn	1.31	6.02		

models, which consider the impacts of erosion, is uneven across different world regions. The main focus is on the global north (with a few exceptions), with severe under-representation of models suitable for ecosystems in Africa and the Middle East, and to a lesser extent, central and South America and Asia (except China). Notably, these regions are at risk of increased erosion and contribute equally with developed regions to calculate the global climate change mitigation potential of SOC sequestration. This study presents an effective model with higher data availability at a regional scale and more diverse spatial heterogeneity for these regions. It can be used to assess changes in soil carbon storage and land-atmosphere carbon exchange due to anthropogenic influences on erosion.

4.3 Uncertainty and limitation

Despite the robust data sources and simulation methods employed in this study, limitations still existed in estimating the spatial distribution of erosion-induced F_L and F_V.

For F_L, it was estimated based on a quantitative assessment of soil loss and sediment transport from hillslopes to rivers. However, due to the limitation of DEM accuracy, the phenomenon of slope attenuation and slope length expansion occurs, which makes the LS factor unable to express the relationship between terrain and soil erosion accurately. Furthermore, the prediction capacity of the sediment transport model was significantly diminished when using observed sediment yields of four sub-basins to calibrate a single coefficient of transport capacity for the whole basin. This finding was confirmed by de Vente et al. (2013) and Borrelli et al. (2018). Additionally, the impact of river management was ignored in this study, as mentioned in section 3.1, further reducing the prediction accuracy. To better fit the simulated sediment yields against observations, separate calibration of transport capacity parameters for each basin or calibration of parameters based on smaller basins without large-scale water conservancy projects is necessary. However, due to the lack of observation data in Dongting Lake Plain, it was challenging to achieve separate calibration in this study. Establishing more sediment monitoring sites for more and smaller basins in the future could develop larger-scale models capable of producing more accurate and realistic simulations of sediment transport.

For F_V, this study ignored the leaching of DOC, which was considered another leak in the terrestrial carbon budget. Zhang et al. (2022) showed that 0.3% of particulate organic carbon decayed into DOC in Europe. Yue et al. (2016) also roughly estimated that the DOC leaching potential accounted for 0.02% of erosion-induced CO_2 flux in the eroded area in China. Since erosion had little effect on DOC, it was disregarded in this study. Furthermore, Lal (2019) indicated that other greenhouse gases, like CH_4 and N_2O, should be considered when exploring the impact of accelerated erosion. These factors should be incorporated into future research. Although this study had limitations, the results were obtained from the most reliable publicly available datasets, and the models implemented in this study promptly assessed carbon loss caused by erosion at the basin scale.

5. Conclusions

This study simulated, to the best of our knowledge, the most complete transfer processes of SOC based on the erosion process model at the basin scale. This model estimates the erosion-induced lateral transport of SOC from land to river systems and the land-atmosphere CO_2 fluxes in the eroded district, depositional district, and transport process. Our findings emphasize the need to simulate the spatial variation of SOC dynamics and stratify calibration and validation. Applying this model to the Dongting Lake Basin, the results showed that 5.18×10^{11} g C a^{-1} would be lost in the riverine system in 1980–2020, only accounting for 12% of the SOC displacement. A large surplus was deposited downslope at foot slopes and flood plains. The erosion-induced CO_2 uptake was 5.54×10^{11} g C a^{-1} in the Dongting Lake Basin during the 40 years. The net influence of water erosion on carbon cycling acts as a terrestrial sink for atmospheric CO_2 at the basin scale. After large-scale ecological restoration in Dongting Lake Basin, the recovery CO_2 sink exceeded the organic carbon lost to riverine systems. In particular, grassland showed the fastest improvement in soil carbon sequestration capacity. Although the model still has limitations on observed data, knowledge gaps in the mechanisms, and scaling methods, this study is helpful in exploring natural and anthropogenic factors affecting SOC dynamics and further provides advice for land management and tillage practices.

Acknowledgements *Acknowledgment for the data support from "National Earth System Science Data Center, National Science & Technology Infrastructure of China. (http://www.geodata.cn)". This work was supported by the National Natural Science Foundation of China (Grant No. U19A2047) and the Natural Science Foundation of Hunan Province (Grant No. 2023JJ20030).*

Conflict of interest The authors declare that they have no conflict of interest.

References

Amelung W, Bossio D, de Vries W, Kögel-Knabner I, Lehmann J, Amundson R, Bol R, Collins C, Lal R, Leifeld J, Minasny B, Pan G, Paustian K, Rumpel C, Sanderman J, van Groenigen J W, Mooney S, van Wesemael B, Wander M, Chabbi A. 2020. Towards a global-scale soil climate mitigation strategy. Nat Commun, 11: 5427

Ananyeva K, Wang W, Smucker A J M, Rivers M L, Kravchenko A N. 2013. Can intra-aggregate pore structures affect the aggregate's effec-

tiveness in protecting carbon? Soil Biol Biochem, 57: 868–875
Andrén O, Kätterer T. 1997. Icbm: The introductory carbon balance model for exploration of soil carbon balances. Ecol Appl, 7: 1226–1236
Baatz R, Hendricks Franssen H J, Euskirchen E, Sihi D, Dietze M, Ciavatta S, Fennel K, Beck H, De Lannoy G, Pauwels V R N, Raiho A, Montzka C, Williams M, Mishra U, Poppe C, Zacharias S, Lausch A, Samaniego L, Van Looy K, Bogena H, Adamescu M, Mirtl M, Fox A, Goergen K, Naz B S, Zeng Y, Vereecken H. 2021. Reanalysis in Earth system science: Toward terrestrial ecosystem reanalysis. Rev Geophys, 59: e2020RG000715
Borrelli P, Paustian K, Panagos P, Jones A, Schütt B, Lugato E. 2016. Effect of good agricultural and environmental conditions on erosion and soil organic carbon balance: A national case study. Land Use Policy, 50: 408–421
Borrelli P, Robinson D A, Fleischer L R, Lugato E, Ballabio C, Alewell C, Meusburger K, Modugno S, Schütt B, Ferro V, Bagarello V, Oost K V, Montanarella L, Panagos P. 2017. An assessment of the global impact of 21st century land use change on soil erosion. Nat Commun, 8: 2013
Borrelli P, van Oost K, Meusburger K, Alewell C, Lugato E, Panagos P. 2018. A step towards a holistic assessment of soil degradation in Europe: Coupling on-site erosion with sediment transfer and carbon fluxes. Environ Res, 161: 291–298
Chaopricha N T, Marín-Spiotta E. 2014. Soil burial contributes to deep soil organic carbon storage. Soil Biol Biochem, 69: 251–264
Chappell A, Webb N P, Viscarra Rossel R A, Bui E. 2014. Australian net (1950s–1990) soil organic carbon erosion: Implications for CO_2 emission and land-atmosphere modelling. Biogeosciences, 11: 5235–5244
de Nijs E A, Cammeraat E L H. 2020. The stability and fate of soil organic carbon during the transport phase of soil erosion. Earth-Sci Rev, 201: 103067
de Vente J, Poesen J, Verstraeten G, Govers G, Vanmaercke M, Van Rompaey A, Arabkhedri M, Boix-Fayos C. 2013. Predicting soil erosion and sediment yield at regional scales: Where do we stand? Earth-Sci Rev, 127: 16–29
Dialynas Y G, Bastola S, Bras R L, Marin-Spiotta E, Silver W L, Arnone E, Noto L V. 2016. Impact of hydrologically driven hillslope erosion and landslide occurrence on soil organic carbon dynamics in tropical watersheds. Water Resour Res, 52: 8895–8919
Dlugoß V, Fiener P, van Oost K, Schneider K. 2012. Model based analysis of lateral and vertical soil carbon fluxes induced by soil redistribution processes in a small agricultural catchment. Earth Surf Processes Landf, 37: 193–208
Doetterl S, Berhe A A, Nadeu E, Wang Z, Sommer M, Fiener P. 2016. Erosion, deposition and soil carbon: A review of process-level controls, experimental tools and models to address C cycling in dynamic landscapes. Earth-Sci Rev, 154: 102–122
Duan X, Bai Z, Rong L, Li Y, Ding J, Tao Y, Li J, Li J, Wang W. 2020. Investigation method for regional soil erosion based on the Chinese Soil Loss equation and high-resolution spatial data: Case study on the mountainous Yunnan Province, China. Catena, 184: 104237
Fontaine S, Barot S, Barré P, Bdioui N, Mary B, Rumpel C. 2007. Stability of organic carbon in deep soil layers controlled by fresh carbon supply. Nature, 450: 277–280
Friedlingstein P, O'Sullivan M, Jones M W, Andrew R M, Gregor L, Hauck J, Le Quéré C, Luijkx I T, Olsen A, Peters G P, Peters W, Pongratz J, Schwingshackl C, Sitch S, Canadell J G, Ciais P, Jackson R B, Alin S R, Alkama R, Arneth A, Arora V K, Bates N R, Becker M, Bellouin N, Bittig H C, Bopp L, Chevallier F, Chini L P, Cronin M, Evans W, Falk S, Feely R A, Gasser T, Gehlen M, Gkritzalis T, Gloege L, Grassi G, Gruber N, Gürses Ö, Harris I, Hefner M, Houghton R A, Hurtt G C, Iida Y, Ilyina T, Jain A K, Jersild A, Kadono K, Kato E, Kennedy D, Klein Goldewijk K, Knauer J, Korsbakken J I, Landschützer P, Lefèvre N, Lindsay K, Liu J, Liu Z, Marland G, Mayot N, McGrath M J, Metzl N, Monacci N M, Munro D R, Nakaoka S I, Niwa Y, O'Brien K, Ono T, Palmer P I, Pan N, Pierrot D, Pocock K, Poulter B, Resplandy L, Robertson E, Rödenbeck C, Rodriguez C, Rosan T M, Schwinger J, Séférian R, Shutler J D, Skjelvan I, Steinhoff T, Sun Q, Sutton A J, Sweeney C, Takao S, Tanhua T, Tans P P, Tian X, Tian H, Tilbrook B, Tsujino H, Tubiello F, van der Werf G R, Walker A P, Wanninkhof R, Whitehead C, Willstrand Wranne A, Wright R, Yuan W, Yue C, Yue X, Zaehle S, Zeng J, Zheng B. 2022. Global carbon budget 2022. Earth Syst Sci Data, 14: 4811–4900
Guenet B, Danger M, Harrault L, Allard B, Jauset-Alcala M, Bardoux G, Benest D, Abbadie L, Lacroix G. 2013. Fast mineralization of land-born C in inland waters: First experimental evidences of aquatic priming effect. Hydrobiologia, 721: 35–44
Harden J W, Sharpe J M, Parton W J, Ojima D S, Fries T L, Huntington T G, Dabney S M. 1999. Dynamic replacement and loss of soil carbon on eroding cropland. Glob Biogeochem Cycle, 13: 885–901
Hoffmann T, Schlummer M, Notebaert B, Verstraeten G, Korup O. 2013. Carbon burial in soil sediments from Holocene agricultural erosion, Central Europe. Glob Biogeochem Cycle, 27: 828–835
Huang N, Wang L, Song X P, Black T A, Jassal R S, Myneni R B, Wu C, Wang L, Song W, Ji D, Yu S, Niu Z. 2020. Spatial and temporal variations in global soil respiration and their relationships with climate and land cover. Sci Adv, 6: eabb8508
Izaurralde R C, Williams J R, Post W M, Thomson A M, McGill W B, Owens L B, Lal R. 2007. Long-term modeling of soil C erosion and sequestration at the small watershed scale. Clim Change, 80: 73–90
Nash J E, Sutcliffe J V. 1970. River flow forecasting through conceptual models part I—A discussion of principles. J Hydrol, 10: 282–290
Jain M K, Das D. 2009. Estimation of sediment yield and areas of soil erosion and deposition for watershed prioritization using GIS and remote sensing. Water Resour Manage, 24: 2091–2112
Jiang M, Medlyn B E, Drake J E, Duursma R A, Anderson I C, Barton C V M, Boer M M, Carrillo Y, Castañeda-Gómez L, Collins L, Crous K Y, De Kauwe M G, dos Santos B M, Emmerson K M, Facey S L, Gherlenda A N, Gimeno T E, Hasegawa S, Johnson S N, Kännaste A, Macdonald C A, Mahmud K, Moore B D, Nazaries L, Neilson E H J, Nielsen U N, Niinemets Ü, Noh N J, Ochoa-Hueso R, Pathare V S, Pendall E, Pihlblad J, Piñeiro J, Powell J R, Power S A, Reich P B, Renchon A A, Riegler M, Rinnan R, Rymer P D, Salomón R L, Singh B K, Smith B, Tjoelker M G, Walker J K M, Wujeska-Klause A, Yang J, Zaehle S, Ellsworth D S. 2020. The fate of carbon in a mature forest under carbon dioxide enrichment. Nature, 580: 227–231
Kirkels F M S A, Cammeraat L H, Kuhn N J. 2014. The fate of soil organic carbon upon erosion, transport and deposition in agricultural landscapes — A review of different concepts. Geomorphology, 226: 94–105
Kwang J S, Thaler E A, Larsen I J. 2023. The future of soils in the midwestern United States. Earths Future, 11: e2022EF003104
Lal R. 2003. Soil erosion and the global carbon budget. Environ Int, 29: 437–450
Lal R. 2004. Soil carbon sequestration impacts on global climate change and food security. Science, 304: 1623–1627
Lal R. 2019. Accelerated soil erosion as a source of atmospheric CO_2. Soil Tillage Res, 188: 35–40
Lal R, Pimentel D. 2008. Soil erosion: A carbon sink or source? Science, 319: 1040–1042
Li J, Liu X, Pan A. 1995. Material erosion, removal and its final arrangement in the rivers of Dongting Lake water system (in Chinese). J Soil Water Conser, 9: 19–27
Li Z, Li X, Zhou S, Yang X, Fu Y, Miao C, Wang S, Zhang G, Wu X, Yang

C, Deng Y. 2022. A comprehensive review on coupled processes and mechanisms of soil-vegetation-hydrology, and recent research advances. Sci China Earth Sci, 65: 2083–2114
Lin J, Guan Q, Tian J, Wang Q, Tan Z, Li Z, Wang N. 2020. Assessing temporal trends of soil erosion and sediment redistribution in the Hexi Corridor region using the integrated RUSLE-TLSD model. Catena, 195: 104756
Liu B, Liang Y, Cao L, Guo Q. 2018. Grid Data on Soil Erodibility in China. In: N.E.S.S.D.C. Loess Plateau Data Center, National Science & Technology Infrastructure
Liu S, Bliss N, Sundquist E, Huntington T G. 2003. Modeling carbon dynamics in vegetation and soil under the impact of soil erosion and deposition. Glob Biogeochem Cycle, 17: 1074
Lugato E, Paustian K, Panagos P, Jones A, Borrelli P. 2016. Quantifying the erosion effect on current carbon budget of European agricultural soils at high spatial resolution. Glob Change Biol, 22: 1976–1984
Nadeu E, Gobin A, Fiener P, van Wesemael B, van Oost K. 2015. Modelling the impact of agricultural management on soil carbon stocks at the regional scale: The role of lateral fluxes. Glob Change Biol, 21: 3181–3192
Naipal V, Lauerwald R, Ciais P, Guenet B, Wang Y. 2020. CE-DYNAM (v1): A spatially explicit process-based carbon erosion scheme for use in Earth system models. Geosci Model Dev, 13: 1201–1222
Panagos P, Borrelli P, Poesen J, Ballabio C, Lugato E, Meusburger K, Montanarella L, Alewell C. 2015. The new assessment of soil loss by water erosion in Europe. Environ Sci Policy, 54: 438–447
Parton W J, Schimel D S, Cole C V, Ojima D S. 1987. Analysis of factors controlling soil organic matter levels in great plains grasslands. Soil Sci Soc Amer J, 51: 1173–1179
Piao S, He Y, Wang X, Chen F. 2022. Estimation of China's terrestrial ecosystem carbon sink: Methods, progress and prospects. Sci China Earth Sci, 65: 641–651
Quinton J N, Govers G, van Oost K, Bardgett R D. 2010. The impact of agricultural soil erosion on biogeochemical cycling. Nat Geosci, 3: 311–314
Ramesh T, Bolan N S, Kirkham M B, Wijesekara H, Kanchikerimath M, Srinivasa Rao C, Sandeep S, Rinklebe J, Ok Y S, Choudhury B U, Wang H, Tang C, Wang X, Song Z, Freeman Ii O W. 2019. Chapter One—Soil organic carbon dynamics: Impact of land use changes and management practices: A review. In: Sparks D L, ed. Advances in Agronomy. London: Academic Press. 1–107
Ran L, Lu X X, Xin Z. 2014. Erosion-induced massive organic carbon burial and carbon emission in the Yellow River basin, China. Biogeosciences, 11: 945–959
Regnier P, Resplandy L, Najjar R G, Ciais P. 2022. The land-to-ocean loops of the global carbon cycle. Nature, 603: 401–410
Scharlemann J P W, Tanner E V J, Hiederer R, Kapos V. 2014. Global soil carbon: Understanding and managing the largest terrestrial carbon pool. Carbon Manage, 5: 81–91
Schimel D S, House J I, Hibbard K A, Bousquet P, Ciais P, Peylin P, Braswell B H, Apps M J, Baker D, Bondeau A, Canadell J, Churkina G, Cramer W, Denning A S, Field C B, Friedlingstein P, Goodale C, Heimann M, Houghton R A, Melillo J M, Moore Iii B, Murdiyarso D, Noble I, Pacala S W, Prentice I C, Raupach M R, Rayner P J, Scholes R J, Steffen W L, Wirth C. 2001. Recent patterns and mechanisms of carbon exchange by terrestrial ecosystems. Nature, 414: 169–172
Schmidt M W I, Torn M S, Abiven S, Dittmar T, Guggenberger G, Janssens I A, Kleber M, Kögel-Knabner I, Lehmann J, Manning D A C, Nannipieri P, Rasse D P, Weiner S, Trumbore S E. 2011. Persistence of soil organic matter as an ecosystem property. Nature, 478: 49–56
Sitch S, Huntingford C, Gedney N, Levy P E, Lomas M, Piao S L, Betts R, Ciais P, Cox P, Friedlingstein P, Jones C D, Prentice I C, Woodward F I. 2008. Evaluation of the terrestrial carbon cycle, future plant geography and climate-carbon cycle feedbacks using five Dynamic Global Vegetation Models (DGVMs). Glob Change Biol, 14: 2015–2039
Stallard R F. 1998. Terrestrial sedimentation and the carbon cycle: Coupling weathering and erosion to carbon burial. Glob Biogeochem Cycle, 12: 231–257
Stewart C E, Paustian K, Conant R T, Plante A F, Six J. 2007. Soil carbon saturation: Concept, evidence and evaluation. Biogeochemistry, 86: 19–31
Tan Z, Leung L R, Li H Y, Tesfa T, Zhu Q, Huang M. 2020. A substantial role of soil erosion in the land carbon sink and its future changes. Glob Change Biol, 26: 2642–2655
Teng H, Chen S, Luo Z, Shi Z, Zhou Y, Wan D, Yao H. 2022. Drivers of water erosion-induced lateral soil carbon loss on the Tibetan Plateau. Catena, 211: 105970
Tifafi M, Guenet B, Hatté C. 2018. Large differences in global and regional total soil carbon stock estimates based on SoilGrids, HWSD, and NCSCD: Intercomparison and evaluation based on field data from USA, England, Wales, and France. Glob Biogeochem Cycle, 32: 42–56
van Oost K, Govers G, Quine T A, Heckrath G, Olesen J E, de Gryze S, Merckx R. 2005. Landscape-scale modeling of carbon cycling under the impact of soil redistribution: The role of tillage erosion. Glob Biogeochem Cycle, 19: GB4014
van Oost K, Quine T A, Govers G, De Gryze S, Six J, Harden J W, Ritchie J C, McCarty G W, Heckrath G, Kosmas C, Giraldez J V, Marques da Silva J R, Merckx R. 2007. The impact of agricultural soil erosion on the global carbon cycle. Science, 318: 626–629
van Oost K, Verstraeten G, Doetterl S, Notebaert B, Wiaux F, Broothaerts N, Six J. 2012. Legacy of human-induced C erosion and burial on soil-atmosphere C exchange. Proc Natl Acad Sci USA, 109: 19492–19497
Verstraeten G, Prosser I P, Fogarty P. 2007. Predicting the spatial patterns of hillslope sediment delivery to river channels in the Murrumbidgee catchment, Australia. J Hydrol, 334: 440–454
Wang J, Feng L, Palmer P I, Liu Y, Fang S, Bösch H, O'Dell C W, Tang X, Yang D, Liu L, Xia C Z. 2020. Large Chinese land carbon sink estimated from atmospheric carbon dioxide data. Nature, 586: 720–723
Wang K, Bastos A, Ciais P, Wang X, Rödenbeck C, Gentine P, Chevallier F , Humphrey V W, Huntingford C, O'Sullivan M, Seneviratne S I, Sitch S, Piao S. 2022. Regional and seasonal partitioning of water and temperature controls on global land carbon uptake variability. Nat Commun, 13: 3469
Wang L, Li Z, Wang D, Hu X, Ning K. 2020. Self-organizing map network-based soil and water conservation partitioning for small watersheds: case study conducted in Xiaoyang Watershed, China. Sustainability, 12: 2126
Wang L, Li Z, Wang D, Chen J, Liu Y, Nie X, Zhang Y, Ning K, Hu X. 2021. Unbalanced social-ecological development within the Dongting Lake basin: Inspiration from evaluation of ecological restoration projects. J Clean Prod, 315: 128161
Wang L, Li Z, Wang D, Liao S S, Nie X, Liu Y. 2022. Factors controlling soil organic carbon with depth at the basin scale. Catena, 217: 106478
Wang X, Xiao X, Qin Y, Dong J, Wu J, Li B. 2022. Improved maps of surface water bodies, large dams, reservoirs, and lakes in China. Earth Syst Sci Data, 14: 3757–3771
Wang Z, Doetterl S, Vanclooster M, van Wesemael B, Van Oost K. 2015. Constraining a coupled erosion and soil organic carbon model using hillslope-scale patterns of carbon stocks and pool composition. J Geophys Res-BioGeoscis, 120: 452–465
Wilken F, Sommer M, Van Oost K, Bens O, Fiener P. 2017. Process-oriented modelling to identify main drivers of erosion-induced carbon fluxes. Soil, 3: 83–94

Xu X, Liu J, Zhang S, Li R, Yan C, Wu S. 2018. China multi-period land use land cover remote sensing monitoring data set (CNLUCC). In: C.A. o.S. Data Registration and publishing System of Resources and Environmental Sciences Data Center

Yang Y, Zhu Q, Liu J, Li M, Yuan M, Chen H, Peng C, Yang Z. 2020. Estimating soil organic carbon redistribution in three major river basins of China based on erosion processes. Soil Res, 58: 540–550

Yue Y, Ni J, Ciais P, Piao S, Wang T, Huang M, Borthwick A G L, Li T, Wang Y, Chappell A, Van Oost K. 2016. Lateral transport of soil carbon and land-atmosphere CO_2 flux induced by water erosion in China. Proc Natl Acad Sci USA, 113: 6617–6622

Zeng Y, Fang N, Shi Z. 2020. Effects of human activities on soil organic carbon redistribution at an agricultural watershed scale on the Chinese Loess Plateau. Agric Ecosyst Environ, 303: 107112

Zhang H, Lauerwald R, Regnier P, Ciais P, Van Oost K, Naipal V, Guenet B, Yuan W. 2022. Estimating the lateral transfer of organic carbon through the European river network using a land surface model. Earth Syst Dynam, 13: 1119–1144

(Editorial handling: Ganlin ZHANG)